# Structural and morphological study of Mn, Zn and Zr freeze-dried transition metal acetates

A. Oliveira de Souza[a,*], L. F. da Silva Tupan[b,c], A. Thyago Jensen[d] and A. Paesano Júnior[b]

[a]*Federal University of the West of Bahia, Multidisciplinary Center of Bom Jesus da Lapa,*
*Avenida Manoel Novaes n°1064, CEP 47600-000, Bom Jesus da Lapa-BA, Brazil.*
[b]*Department of Physics, State University of Maringá,*
*Avenida Colombo n°5790, CEP 87020-900, Maringá-PR, Brazil.*
[c]*Uuniversity Center Ingá- Rod Pr 317 n°6114, CEP 87100-000, Maringá-PR, Brazil.*
[d]*Federal University of the West of Bahia, Center for Exact Sciences and Technologies,*
*Rua Bertioga, 892, Morada Nobre I, CEP: 47810-059, Barreiras-BA, Brazil.*

Manganese (II) acetates tetrahydrate, zinc dihydrate and anhydrous zirconium, processed by freeze-drying, were heat-treated in free atmosphere at different temperatures and times, generating the main oxides of these metals. These acetates were structurally characterized by scanning electron microscopy (SEM), thermogravimetry (TG), differential scanning calorimetry (DSC), along with all the oxides generated, by X-ray diffraction (XRD) and UV-VIS difused absorption spectroscopy. Calculations obtained from TG data showed that manganese acetate lost two waters after freeze-drying, also confirmed by X-ray data and that the same phenomenon may be occurring for zinc acetate. The results indicate that exothermic events occurred at lower temperatures for freeze-dried acetates, which may be related to the high surface area of the material, and consequent greater reactivity. The total decomposition temperatures of the acetates in the ZnO and ZrO2 semiconducting oxides and the manganese oxides Mn2O3 and Me3O4, with excellent crystallization, were obtained.

*Keywords:* Freeze-drying; metal acetates; termogravimetry; differential scanning calorimetry; oxide nanostructures.

## 1. Introduction

Recently, one-dimensional (1D) semiconductor oxide nanostructures, such as nanowires, nanorods, and nanotubes, have been the intensive research focus for their potential applications in optical, electrical, optoelectronic, photocatalytic, and hydrophilic/hydrophobic felds [1]. To potentialize the efficiency of these nanodevices in various fields of science, it is a premise to construction of nanostructured materials in two-dimensional (2D) or three-dimensional (3D) structures.

The study of the production and characterization of nanostructured materials - those with size on the order of nanometers and generally smaller than 100 nm - has been extensively explored, because these new nanometric materials have completely different physical and chemical properties when compared to solids macroscopic [2]. These variations in properties result from reduced size, crystallite form, low density and/or coordination number at the interfaces between the structural elements and also due to its large surface area or quantum size effect [3]. Research into these new properties (nanoscience) and associated applications (nanotechnology) is one of the most promising areas of research today. Among these materials, we can mention as nanostructured semiconductors, showing the potential of use in the fields of spintronics [4-6], the conversion of solar energy into electricity with solar cells [7], in electronic optics, electronic devices in nanoscale, light-emitting nanodevices, laser technology, waveguide, chemicals and biosensors [3,8,9].

The nanostructured materials can be obtained by various processes, such as chemical routes, high energy milling, fast solidification, among others. In this study, we will explore the freeze-drying processing of transition metal acetates, followed by thermal treatments, to produce simple or complex, nanostructured oxides.

The freeze-drying is frequently used to dehydrate aqueous mixes resulting in a final product with fine or ultrafine solid particles that maintains the basic structure of the initial salt, which shows high homogeneity and chemical reactivity due to the increase of its surface area [10,11]. Any modification in the mass of the sample is usually related to the water loss.

Metal acetates are highly water soluble salts which can readily decompose into nanostructured oxides by appropriate heat treatments, releasing H2O, acetic acid, acetone and $CO_2$. They are generally used as precursors for the synthesis of numerous compounds with low cost, simplicity and a well-controled process, through controlled chemical reactions or simple one-step solid state reaction of pure acetates or stoichiometric mixtures thereof. The thermal decomposition of acetates, under various conditions of thermal treatments, has attracted the attention of researchers due to the great applicability involving the synthesis of ceramic compounds.

Through freeze-drying followed by thermal treatments of metal acetates, our research group obtained the following nanostructured materials: enriched iron(III) acetate [12], iron acetate (III) anhydrous [13], the dilute magnetic semiconductor oxides $ZrFeO_2$ [14] e CuFeO [15].

TABLE I. Acetates used in the preparation of samples and respective purities.

| Material | Chemical formula | Manufacturer | Purity (% at.) |
|---|---|---|---|
| Manganês(II) acetate tetrahydrate | $Mn(CH_3COO)_2 \cdot 4H_2O$ | Vetec | 99.5 |
| Zinc acetate dihydrate | $Zn(CH_3COO)_2 \cdot 2H_2O$ | Synth | 99.99 |
| Anhydrous zirconium acetate | $Zr(CH_3COO)_4$ | Aldrich | - |

The main objectives of this work are to:

(i) obtain the crystalline solid nanostructured products of zinc acetates (host matrix), zirconium (host matrix) and manganese (dopant) by the freeze-drying process;

(ii) use freeze-drying to reduce the water content of manganese (IV) acetate;

(iii) obtain the pure host matrices of the ZnO and $ZrO_2$ semiconductor oxides;

(iv) make a comparative study of acetates received and freeze-dried;

(v) use freeze-drying process to change the morphology of metal acetates and formed solids.

The acetates (as-received and freeze-dried) were characterized by Scanning Electron Microscopy (SEM), X-ray Diffractometry (XRD) and Thermogravimetry (TG)/Differential Exploratory Calorimetry (DSC).

Thus, the results presented here supply the lack of more focused and condensed studies on the products generated from the thermal decomposition of zinc, zirconium and manganese metal acetates originally processed by freeze-drying.

## 2. Experimental description

### 2.1. Preparation of the samples

The marks are specified in Table I. The acetates received as manganese (AcMn), zirconium (AcZr) and zinc (AcZn) were completely dissolved in approximately 100 ml of water (distilled and deionized) in a beaker at room temperature. They were then freeze-dried.

### 2.2. Freeze-drying

In the freeze-drying process, the homogenous mixture (acetate + water) was placed in a glass bottle, suitable for the freeze-drier equipment (*i.e.*, freeze-drier Liotop brand model -L101) and frozen in liquid nitrogen. The vial was then coupled to the freeze-drier and the solution was dried by sublimation under low pressure ($\sim 250 \ \mu mHg$) and temperature (-$58°C$). The time for the complete drying of the sample lasted approximately 20 hours, after which the sample naturally returned to room temperature. The freeze-dried manganese,

zinc and zirconium acetates will hereinafter be referred to as AcMn-L, AcZn-L and AcZr-L, respectively.

Subsequently, all amorphous and low-density powders obtained by the freeze-drying processwere subjected to free atmosphere heat treatments at different temperatures and times in the case of manganese acetate. Alumina boats were used to support the samples during the heat treatments, which were conducted in a resistive oven (type EDG muffle, EDG10P - S, model 3000) with a heating rate of $10°C$/min., temperatures of $250°C$, $350°C$ and $500°C$ for 1 hour and 3 hours for manganese acetate, $400°C$ for 3 hours for zinc acetate, and $600°C$ for 3 hours for zirconium acetate. At the end of the isothermal stage, the oven was switched off and the samples cooled slowly inside the oven to room temperature ($\sim 27°C$).

### 2.3. Characterization techniques

#### 2.3.1. SEM

The morphological aspect of the studied materials (*i.e.*, AcMn, AcMn-L, AcZn, AcZn-L, AcZr and AcZr-L) was analyzed by SEM in a Shimadzu (SS 550 Superscan) scanning electron microscope, through the formed image by secondary electrons.

#### 2.3.2. TG/DSC

The thermal decomposition of the investigated materials was studied by the TG/DSC techniques (samples with $\sim$ 9 mg mass, contained in an alumina crucible), carried out in a Netzsch thermal analyzer (model STA 409 PG/4/G Luxx), in atmosphere ($N_2 = 80\%$, flow rate 40 ml/min, $O_2 = 20\%$, flow rate 10 ml/min). The empty crucible measurement was used for the reference of the baseline (for both TG and DSC). The temperature was raised from ambient to $500°C$ (AcMn and AcMn-L) and $1200°C$ (AcZn and AcZr), with a heating rate of $10°C$/min.

#### 2.3.3. X-Ray Diffraction

The structure/crystallinity of the freeze-dried and thermally treated acetates (and solids formed) was determined by X-ray diffraction.

The measurements were conducted at room temperature in a Shimadzu diffractometer (model XRD-6000), operating in geometry (*i.e.*, Bragg-Brentano, $\theta - 2\theta$). The radiation used was the K$\alpha$ of the copper tube ($\lambda = 1.54064$ Å), with a

voltage of 40 kV and a current of 30 mA. The diffractograms were taken in a range of $5° \leq 2\theta \leq 90°$, with step of $0.02°$ and counting time of 6 s per step.For some samples, Rietveld refinements were performed with the Fullprof program [16] and the refractive gratings were presented as usually specified in the literature.

The intensity of the peaks indicated according to the ICDD (International Center For Diffraction Data) database.

### 2.3.4. *UV-VIS difused absorption spectroscopy*

The band gap energy of the samples was obtained at room temperature in a UV-VIS spectrophotometer (Ocean Optics USB2000+), using an integrating sphere attachment. A difused absorption spectroscopy measurement in the range of $200 - 800$ nm. The direct optical bandgap of ZnO and $ZrO_2$ was estimated by diffuse reflectance spectra with concentration solution ($0.2$ mg/cm$^3$) and optical path $= 1.0$ cm and analyzed by the Tauc model:

$$\alpha h\gamma = C(h\gamma - Eg)^n,$$

where $C$ is a proportionality constant, $h\gamma$ is the energy of the photon, $\alpha$ is the molar absorption coefficient of the Beer-Lambert law and $n$ is a factor related to the type of electronic transition in the semiconductor [26].

## 3. Results and discussion

### Scanning electron microscopy of acetates

Figure 1 shows the microphotographs of AcZn acetates (Fig. 1a)) and AcZn-L (freeze-dried), Fig. 1b).

It can be observed that the microstructure of both samples presents a very distinct aspect, *i.e.*, in the form of sheets [13,17,18], with thicknesses at nanoscale ($\sim$ 78.1 nm) for AcZn-L acetate and morphology with micrometric agglomerates for AcZn.

The SEM image for AcZr is shown in Fig. 2a), which also shows an appearance of micrometric agglomerates. On the other hand, the micrograph of AcZr-L (freeze-dried), Fig. 2b), has a shape characteristic of flakes in submicron scale.
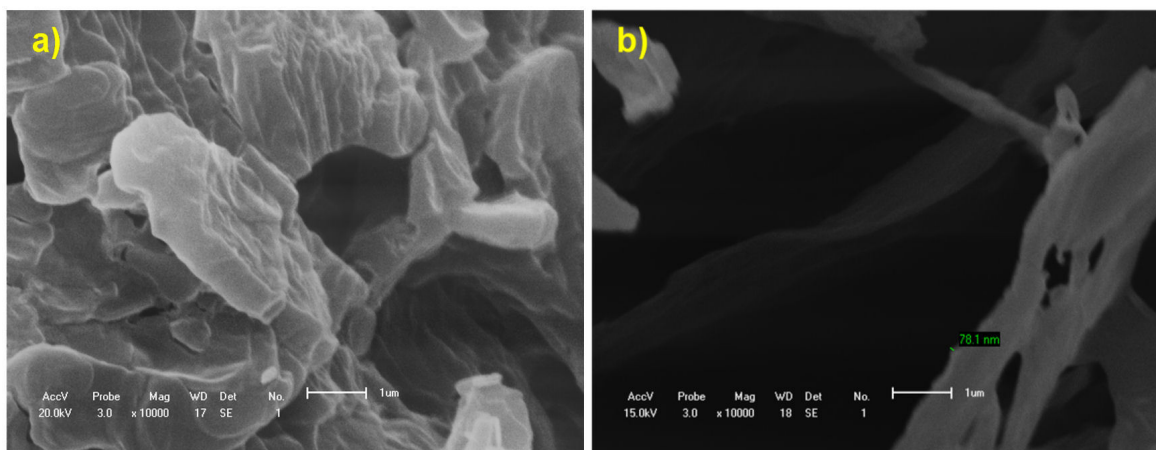


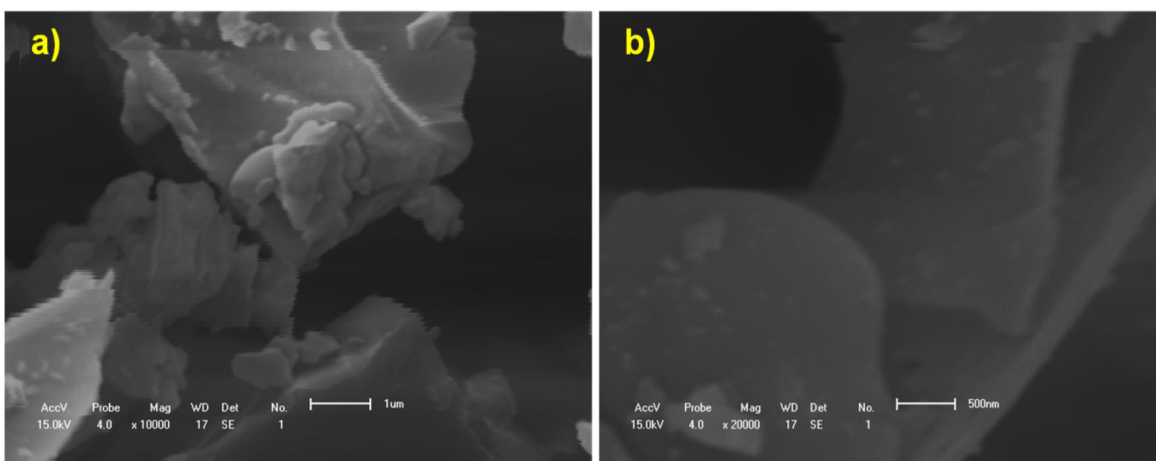FIGURE 1. Microstructure of acetates: a) AcZn and b) AcZn-L.



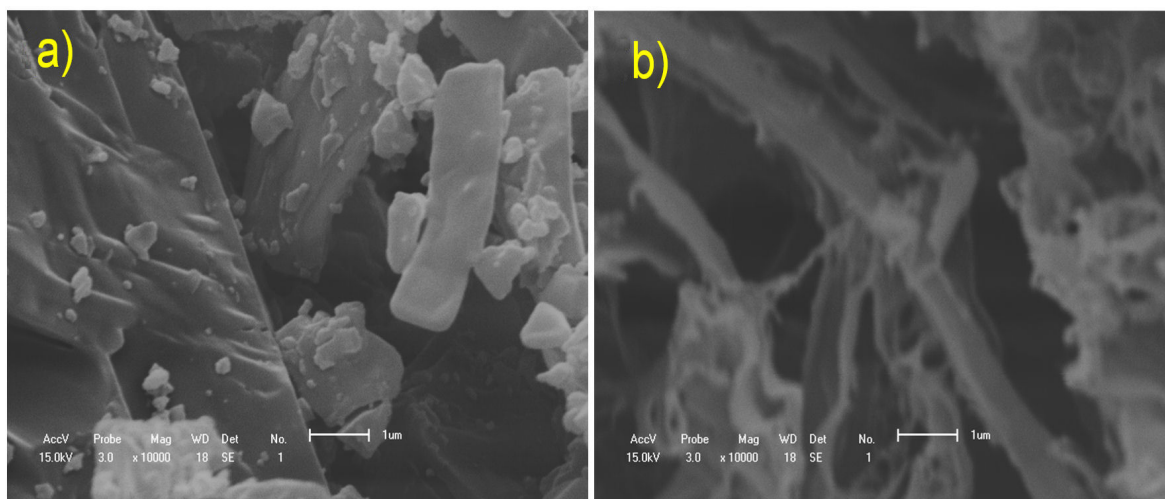FIGURE 2. Microstructures of acetates: a) AcZr and b) AcZr-L.

FIGURE 3. Microstructures of acetates: a) AcMn and b) AcMn-L.

Figure 3 shows micrographs of the AcMn acetates (Fig. 3a)) and AcMn-L (freeze-dried), Fig. 3b). It can be seen that the microstructure of the AcMn sample has a rather irregular appearance, *i.e.*, of indefinite geometry with a micrometer scale thicknesses. On the other hand, the AcMn-L presents microstructure in the form of Sheetsin submicrometric scale.

From these results, it can be inferred that the freeze-drying process reduced the average particle size and shape of the precursors by inserting them in the nanometric scale, which can lead to a change in the chemical and physical properties of the precursors, possibly making them more reactive, according to the DSC/TG data below.

Since there is less water available between the acetate bonds in the freeze-dried material, this change in shape and size may be justified considering that the surface area of the solid product formed is dependent on the availability of water during the dehydration process [19]. In this context, the advantage of freeze-drying is the possibility of preparation of nano or submicrometric escaled homogeneous samples [20] and at lower temperatures [13].

**Diffractometric analyzes**

Figure 4 shows the X-ray diffractograms of the as-received zinc acetate (a) and the freeze-dried material (b). Both show diffraction peaks that can be attributed to the dihydrate acetate $Zn(CH_3COO)_2 \cdot 2H_2O$, according to the record 033-1464 of ICDD.

Different intensities, including the appearance of a peak (indicated by $\pi$) of low intensity at $2\theta = 6.5°$. We believe that, similarly to what happens in the case of freeze-dried manganese acetate (Fig. 6 below), a possible explanation for this difference between the two materials could be due to the fact that the freeze-dried zinc acetate lost structural water during the freeze-drying processing.

Figure 5a) shows diffraction of X-rays for zirconium acetate as-received, then drying at room temperature, once it
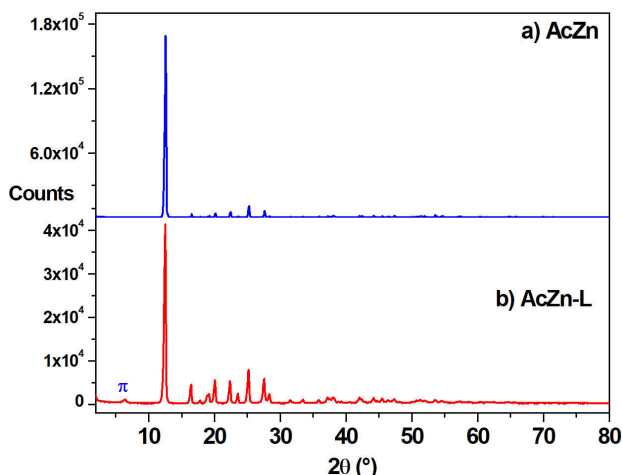


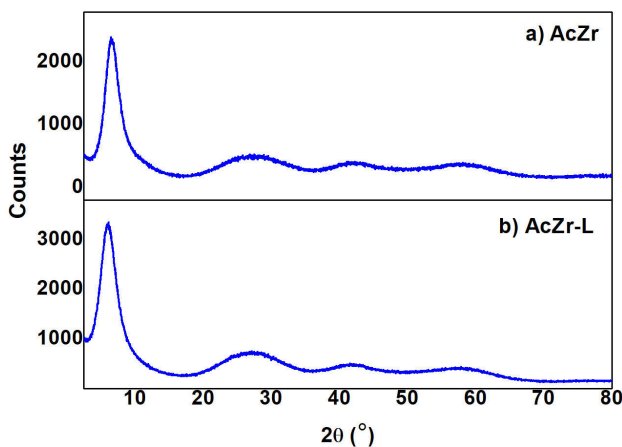FIGURE 4. X-ray diffractograms of a) AcZn and b) AcZn-L.



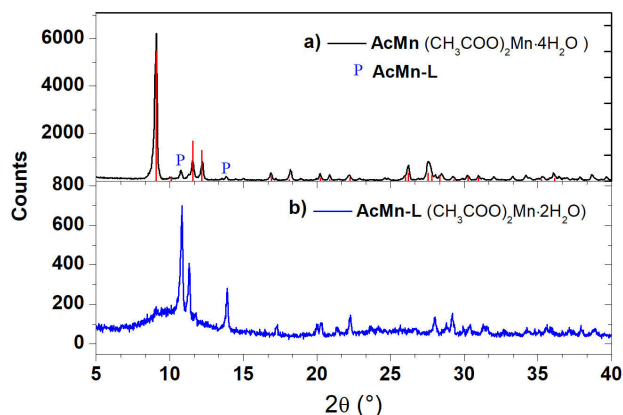FIGURE 5. X-ray diffractograms of Zr acetates a) AcZr and b) AcZr-L.

FIGURE 6. X-ray diffractograms ofMn acetates: a) AcMn and b) AcMn-L.

has been diluted in acetic acid. The Fig. 5b), in turn, refers to AcZr-L and, as it can be observed, there was no structural modifications in relation to AcZr (compared to record 28-1494 of ICDD).

Figure 6a) shows the diffractogram of the AcMn, which shows, in addition to the respective standard for that compound tetrahydrate (compared to record 029-0879 of the ICDD standard), small peaks (indicated by p) which may - as hereinafter disclosed by TG/see Fig. 9 - be attributed to the manganese acetate dihydrate $Mn(CH_3COO)_2 \cdot 2H_2O$. Figure 6b), meanwhile, refers to the AcMn-L and shows a different diffraction pad comparing to the previous one, possibly of the phase (unique) $Mn(CH_3COO)_2 \cdot 2H_2O$, partially amorphized, which we did not find files of ICDD to compare it with.

## 3.1. TG/DSC of acetates

TG/DSC measurements performed simultaneously for the AcZn-L, done under synthetic airflow, are presented in Fig. 7. TG/DSC curves analyses indicate the presence of two important thermal events (I-II).

When observing Fig. 7a), it can be verified that the event I (27-200°C) is associated to the dehydration and evolution of adsorbed gases. After event I, the mass loss of dehydration
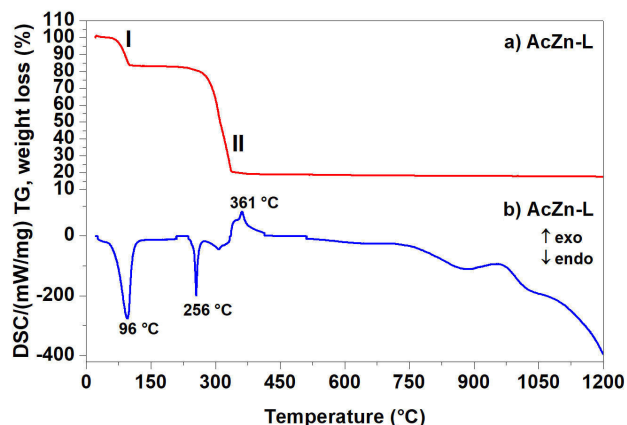
measured at 200°C was 17.2%, which is consistent with the theoretical value 16.4% [21]. The fact that a greater loss of mass for AcZn-L was obtained may be related to an adsorption of water in the AcZn, acquired during the storage of this material in the laboratory.

Figure 7b) shows the DSC curves, where event I (27-200°C) involves endothermic transitions with two peaks (96 and 256°C) for AcZn-L. These endothermic peaks correspond to the dehydration process for these materials.

The TG data of Fig. 7a) indicates that event II (200-400°C) with 80.1% total mass loss, measured at 400°C, represents the thermal decomposition of AcZn-L. The difference between the total mass loss and the mass loss for the decomposition was 62.9%. Typically, the decomposition of the zinc acetate dehydrate $Zn(CH_3COO)_2 \cdot 2H_2O$ leads to the formation of ZnO, with a loss of mass of 62.92%. This value is very close to the experimental data of $\sim$ 62.90% obtained from TG. Therefore, the ZnO phase corresponds to the solid product formed from the decomposition of AcZn-L.

The DSC data of Fig. 7b) indicates that event II (200-440°C) involves multiple steps, with the first two being endotherms and one exotherm at 361°C. This indicates that the dehydrated acetate decomposes completely in the zinc oxide.

The results of TG/DSC for AcZr-L, also performed under synthetic air flow, are shown in Fig. 8. It can be seen that the total mass loss observed at 500°C was 44%. Considering a stoichiometric anhydrous zirconium(IV) acetate, $Zr(CH_3COO)_4$ decomposing to zirconium dioxide, the theoretical mass loss would be 44.4%. Therefore, there is a clear convergence between the experimental and the theoretical results.

It is inferred from Fig. 8b) that the endothermic event, occurring at 78°C, is associated with the decomposition of the organic groups ($H_2O$, acetone, $CO_2$, among others) [22] contained in freeze-dried zirconium acetate. The exothermic event, with a single acute peak well defined at 361°C, corresponds to the thermal decomposition of the compound, which leads to the formation of zirconia.

TG/DSC measurements for manganese acetates, performed under synthetic airflow, are presented in Fig. 9.



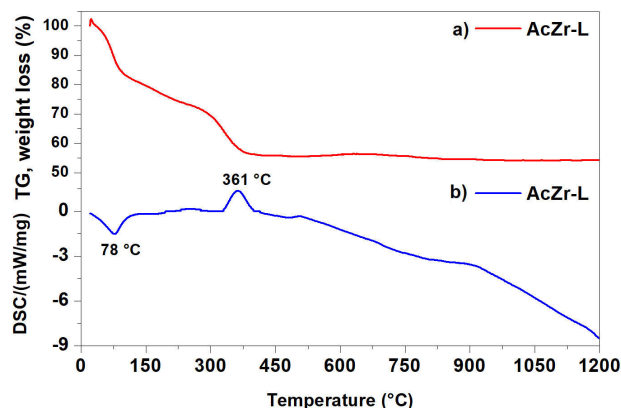FIGURE 7. a) TG and b) DSC curves for AcZn-L powders.



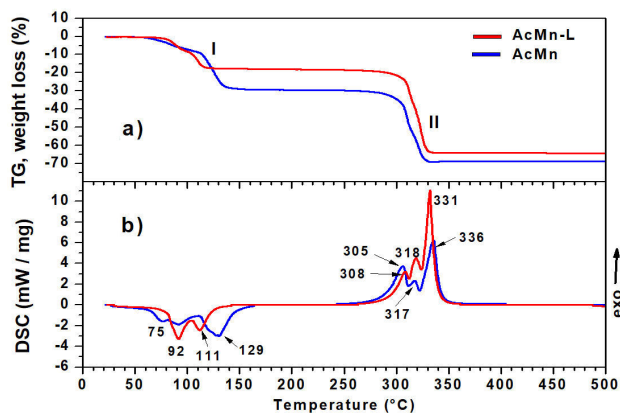FIGURE 8. a) TG and b) DSC curves for AcZr-L powders.

FIGURE 9. a) TG and b) DSC curves for AcMn and AcMn-L powders.

TG/DSC curves analyses indicate the presence of two important thermal events (I-II).

When observing Fig. 9a), it can be verified that the event I (27-200°C) is associated with the loss of structural water, both for the AcMn-L and the as-received AcMn. After event I, the mass loss for the AcMn-L measured at 200°C was 18.2%. Theoretically, the loss of $2H_2O$ corresponds to a mass loss of 17.2% [23]. It can be concluded that, after freeze-drying, the AcMn-L contains two waters in its structure . The mass loss for the AcMn measured at 200°C was 29.4%. Theoretically, the loss of $4H_2O$ would correspond to a mass loss of 34.5% [23]. Calculations performed from TG data for the AcMn indicate that it contains 3.4 H2O in its structure. The comparison of AcMn XRD peaks (Fig. 6a)) with the AcMn-L (Fig. 6b)) indicates that the precursor used (AcMn) may contain a small portion of $Mn(CH_3COO)_2 \cdot 2H_2O$ in its structure. Using the TG data, it was possible to estimate the percentage of the two compounds present ($x = 70\%$ of AcMn·$4H_2O$ and $y = 30\%$ of AcMn·$2H_2O$) in the AcMn, through the relation $x4H_2O + y2H_2O = 3.4H_2O$.

Figure 9b) shows the DSC curves, where event I (27-200°C) involves endothermic transitions with two peaks (92 and 111°C) for the AcMn-L, and three peaks (75, 92 and 129°C) for the AcMn system. These endothermic peaks correspond to the dehydration process for these materials. The presence of three peaks for the AcMn indicates a more complex process for the release of the structural waters (30% AcMn·$2H_2O$ + 70% AcMn·$4H_2O$), compared to the AcMn-L ($\sim 100\%$ Mn·$2H_2O$).

TG data of Fig. 9a) indicate that event II (200-500°C), with 64.1% total mass loss for the AcMn-L and 68.6% total loss of the AcMn, both measured at 400°C, represent the thermal decomposition of the sample. The difference between the total mass loss and the mass loss for the decomposition was 45.9% for the AcMn-L and 39.2% for the AcMn. Theoretically, the decomposition of the dehydrated manganese acetate ($Mn(CH_3COO)_2$, symbol AcMn-D) leads to the formation of $Mn_2O_3$, with a mass loss of 45.6%. This value is very close to the experimental data of 45.9% obtained from TG. Therefore, the $Mn_2O_3$ phase corresponds to the solid product of the decomposition of the AcMn-D. The fact that 39.2% of the mass loss was obtained for the decomposition of the AcMn could correspond to the formation of a mixture of oxides containing $Mn_2O_3$ (majority) and $Mn_2O_4$ (minority). This characteristic can be related to the morphology of the powder, with this one composed by more compacted agglomerates in comparison to the AcMn-L, which presented itself as more reactive (containing an amorphous portion observed to the XRD). Therefore, $Mn_2O_4$ could be considered an intermediate phase for the formation of $Mn_2O_3$, even in the AcMn.

DSC data from Fig. 9b) indicate that event II (200-500°C) involves exothermic transitions with three peaks (308, 318 and 331°C) for the AcMn-L, whereas there are three peaks (305, 317 and 336°C) for the AcMn. This indicates that both dehydrated acetates decompose in much the same way,
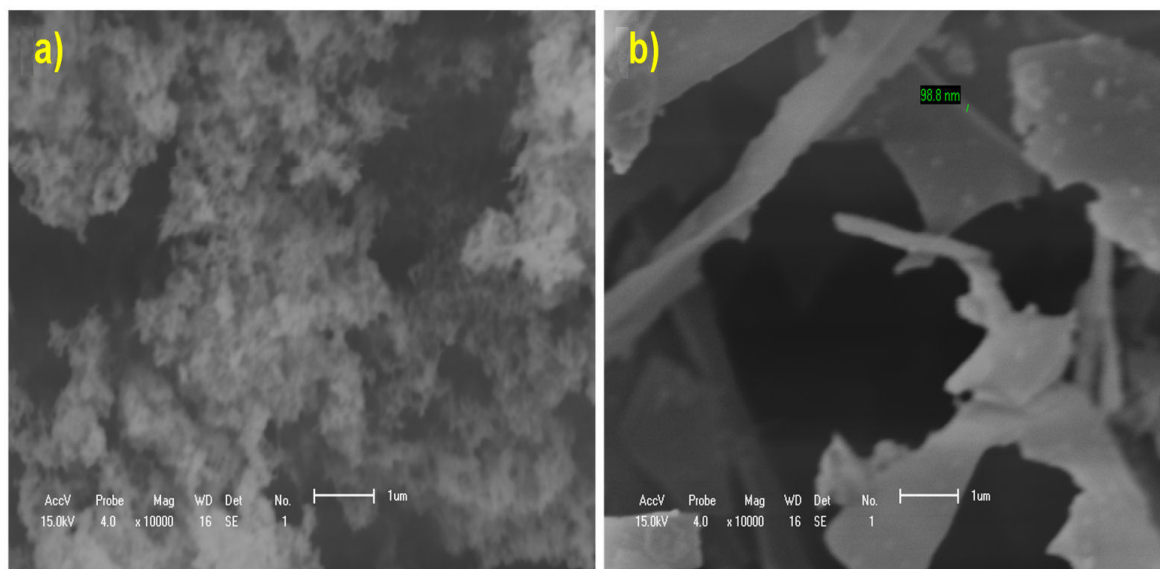


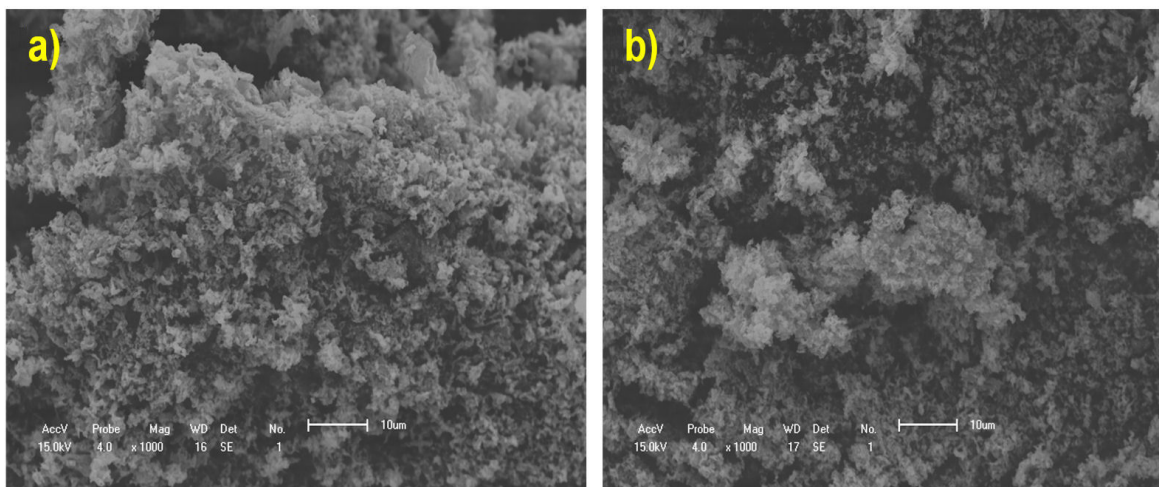FIGURE 10. Semiconductor microstructures: a) ZnO and b) $ZrO_2$.

FIGURE 11. Microstructures of manganese oxides: a) $Mn_3O_4$ and b) $Mn_2O_3$.

## 3.2. SEM of the solid products formed

The low-resolution SEM image for synthesized ZnO (*i.e.*, obtained by the heat treatment of AcZn-L at 400°C for 3 hours) is shown in Fig. 10a), which does not allow a definition of the form of the agglomerates with high porosity. However, the micrograph of as-synthesized $ZrO_2$ (obtained by the heat treatment of AcZr-L for 3 h at 600°C free atmosphere), in Fig. 10b), has nanoplates at nanoscale ($\sim$ 98 nm) as its characteristic shape. It is worth mentioning that even after the heat treatment for the formation of zirconium oxide, the nanoplates formed by the freeze-drying process were still maintained.

From the SEM results, it is possible to see that the microstructures of Mn3O4 oxides (Fig. 11a)) and $Mn_2O_3$ (Fig. 11b)) are very similar to agglomerates with high porosityat submicron scales [24].
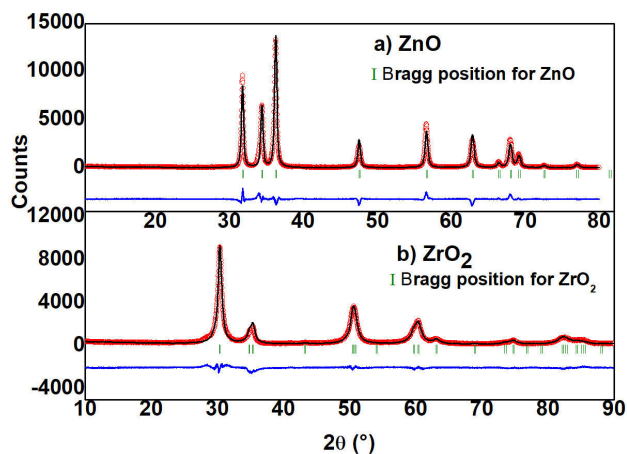


FIGURE 12. X-ray diffractograms of as-synthesized ceramics: a) ZnO and b) $ZrO_2$.

## 3.3. DRX of thermally treated acetates

From the initial study with the thermal analysis, it was possible to find a temperature range to obtain the main solids formed with the transition metal acetates.

Figure 12 shows the diffractometric data, refined by Rietveld, for the obtained semiconductor oxides. In Fig. 12a), the X-ray diffractogram belonging to the as-synthesized ZnO can be seen. It is verified that it presents a single pattern, relative to the compact hexagonal structure (wurtzita), with space group $P_{63}mc$, compared to the file 089-7102 of the ICDD. Figure 12b) shows the as-synthesized tetragonal $ZrO_2$ spectrum, which also exhibits a unique zirconia pattern with spatial group $P_{42}/nmc$, compared to the ICDD datasheet 049-1642. The structural parameters found in the refinements are in full agreement with the values established in the respective ICDD files.

Figure 13 shows the diffractograms of manganese acetate freeze-dried and thermally treated in free atmosphere at different times and temperatures.

The diffractogram of Fig. 13a) refers to the AcMn-L, treated at the temperature of 250°C for 1 h. As it can be verified, this result shows the partial decomposition of AcMn-L, resulting in hausmanite ($Mn_3O_4$, major phase) and manganese carbonyl ($C_{10}Mn_2O_{10}$, minority phase).

The sample AcMn-L also treated at 250°C, but for 3 h (Fig. 13b)) only provides the diffraction profile of $Mn_3O_4$ (record 080-0382 of the ICDD standard). It can be concluded from this result that the decomposition of the manganese carbonyl also resulted in $Mn_3O_4$ (with the structure of hausmannite), which becomes the single component of the sample.

Figure 13c shows the diffractogram for the AcMn-L, heat-treated at 350°C for 1 h. For this condition, it was found that the acetate decomposed into manganosite (MnO) minor phase and $Mn_3O_4$ (majority).
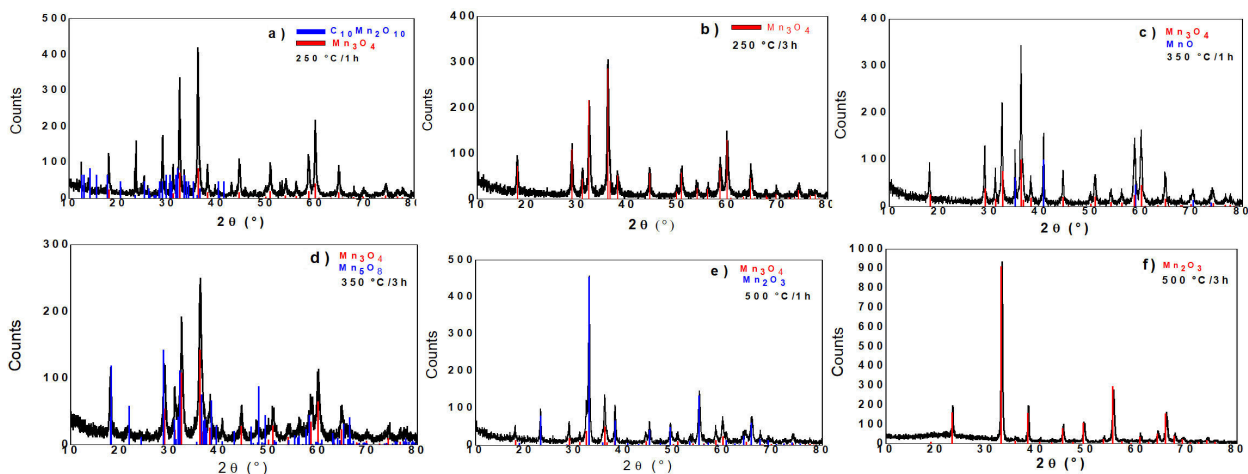
FIGURE 13. Diffractograms of the thermally treated AcMn-L in: a) 250°C/1 h, b) 250°C/3 h, c) 350°C/1 h, d) 350°C/3 h, e) 500°C/1 h and f) 500°C/3 h.

Figure 13d) refers to the treated AcMn-L at 350°C for 3 h. As noted, the longer heat treatment gave rise to manganese oxide ($Mn_5O_8$), accompanied by $Mn_3O_4$. According to the literature, hausmanite effectively oxidizes to bixbyite when heated/treated above 400°C, whereas for lower temperatures there is formation of the $Mn_5O_8$ phase, intermediate to $Mn_3O_4$ and $Mn_2O_4$. In all cases, at temperatures higher than 400°C, $Mn_5O_8$ totally becomes $Mn_2O_4$ [25].

In the observation of the XRD of the AcMn-L sample treated at 500°C for 1 h (Fig. 13e)), the absence of peaks re-lated to manganosite is verified. It is assumed that, at this temperature, the manganosite is decomposing into $Mn_2O_3$ (bixbyite), giving indications that in the vicinity of 500°C the sesquioxide becomes the major constituent, according to the TG data already discussed.

The X-ray pattern of the AcMn-L sample treated at 500°C for 3 h (Fig. 13f)) perfectly provides the diffraction profile of $Mn_2O_3$ (ICDD standard sheet 071-0636). It is possible to associate this result with the transformation of hausmanite and $Mn_5O_8$ completely into bixbyite, which becomes the single phase of the sample. Thus, the $Mn_2O_3$ phase is the most stable manganese oxide at this temperature and time, which is in agreement with the TG data already discussed.

As previously observed, the heat treatment of AcMn-L caused the organic matter of the acetate to be converted to oxides. Thus, the various phases of the decomposition of manganese acetate are attributed to the variety of manganese oxidation states, allowing the formation of oxides with many different stoichiometries and most of them with antiferro-magnetic behavior.

### 3.4. UV-VIS

From the UV-VIS absorption spectra, the band gap values were calculated for the ZnO and $ZrO_2$ , using the linear extrapolation of the Tauc graphs (Fig. 14a-b)).

The band gap value for ZnO is 3.26 eV, which is close to the value reported in the literature [27]. And to $ZrO_2$ the band gap value is 5.42 eV [28], These values confirm that the synthesis route is also effective in terms of preserving semiconductor properties as material values.

### 4. Conclusions

The pure crystalline phases of the semiconductor oxides of ZnO and $ZrO_2$ and of the oxides of $Mn_2O_3$ and $Mn_3O_4$ of the zinc, zirconium and manganese acetates, respectively, were obtained by freeze-drying processing, followed by thermal
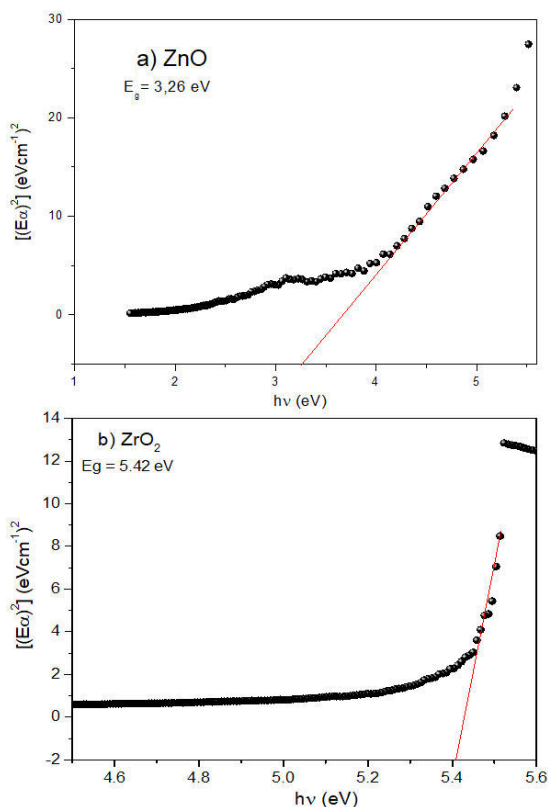


FIGURE 14. Tauc's graph of the a) ZnO and b) $ZrO_2$ system.

treatments. For these solid products, the exact temperatures of total decomposition of the aforementioned acetates obtained were: 250°C for 3 hours forms $Mn_3O_4$; 500°C for 3 hours, $Mn_2O_3$; 400°C for 3 hours, ZnO; and 600°C for 3 hours, the $ZrO_2$. With the data of DSC/TG, DRX and UV-VIS it was possible to verify that, after the freeze-drying, the number of structural water of manganese acetate was reduced. The results of the present investigation reveal that the freeze-drying process caused a morphological alteration in the particulate of the compounds, creating submicrometric or nanostructures with high aspect ratio, remaining after heat treatments to form solid products according to SEM data. In the comparative study, it was possible to observe that the freeze-dried material produced solid products at lower temperatures, indicating that the processing by freeze-drying causes a morphological modification in the materials making them more reactive. Taking advantage of the aforementioned characteristics of freeze-dried acetates, it is also possible to synthesize (*i.e.*, freeze-dry and heat treat) a mixture of two (or more) acetates to form a nanometric semiconductor oxide, of stoichiometric composition or, eventually, with the cations of a metal in solid solution in the oxide matrix of another metal.

## Acknowledgments

1. X. Wu, X. Xu, H. Zeng and C. Guo, Self-Assembly of Semiconductor Metal Oxide Nanostructures, *Journal of Nanomaterials*, **2013** (2013) 1-2.

2. R. Valenzuela, *Chemistry of Solid State Materials: Magnetic Ceramics*. (Cambridge University Press, 2005).

3. S. Suresh, Semiconductor Nanomaterials, Methods and Applications: *A Review, Nanoscience and Nanotechnology*, **3** (2013) 62.

4. K. Sato, H. Katayama-Yoshida and P. H. Dederichs, Dilute magnetic semiconductors. *Scientific Highlight of the Month*, **75** (2010) 93.

5. J. Stankiewicz, Diluted magnetic semiconductors. *Third Brazilian School of Semiconductor Physics*, **3** (1987) 281.

6. J. K. Furdyna, Diluted magnetic semiconductors: An interface of semiconductor physics and magnetism (invited). *J. Appl. Phys.*, **53** (1982) 7637.

7. J. A. Anta, E. Guillé, and R. Tena-Zaera, ZnO-based dye-sensitized solar cells. *J. Phys. Chem. C*, **116** (2012) 11413. https://doi.org/10.1021/jp3010025.

8. V. Agrahari, M. C. Mathpal, M. Kumar, and Agarwal. Investigations of optoelectronic properties in DMS SnO2 nanoparticles. *J. Alloys Compd.*, **622** (2015) 48, https://doi.org/10.1016/j.jallcom.2014.10.009.

9. P. Chetri and A. Choudhury, Investigation of optical properties of SnO2 nanoparticles, *Physica E*, **47** (2013) 257, https://doi.org/10.1016/j.physe.2012.11.011.

10. R. Louis, C. M. Joan, *Freeze Drying/Lyophilization of pharmaceutical and Biological products*. Third ed. London: (Informa Healthcare, 2010).

11. O. George-Wilhelm, H. Peter, *Freeze-Drying*. Second ed. Weinheim: (Wiley-VCH, 2004).

12. A. O. de Souza *et al.*, *Nova* **37** (2014) 1132.

13. A. Oliveira de Souza*, V. Biondo, F. Francisco Ivashita, G. C. de Souza Nunes and A. Paesano Jr., Structural and Magnetic Characterization of Nanostructured Iron Acetate. *Orbital: The Electronic Journal of Chemistry*. **09** (2017) 261.

14. A. O. de Souza, F. F. Ivashita, V. Biondo, A. Paesano Jr. and D. H. Mosca, Structural and magnetic properties of iron doped ZrO2, *J. Alloy. Compd* **680** (2016) 701.

15. A. A. Oliveira, M. I. Valerio-Cuadros, L. F. S. Tupan, F. F. Ivashita and A. Paesano Jr., Size-effect on the optical behavior of Fe-doped CuO nanoparticles synthesized by a freeze-drying process, *Materials Letters,* **229** (2018) 327.

16. Rodriguez-Carvajal, J., Short Reference Guide of the Program FULLPROF, http://www-llb.cea.fr/fullweb/powder.htm.

17. S. Biswas, L.T. Drzal, Multilayered Nanoarchitecture of Graphene Nanosheets and Polypyrrole Nanowires for High Performance Supercapacitor Electrodes, *Chem. Mater.* **22** (2010) 5667.

18. C. Wu *et al.*, Twodimensional vanadyl phosphate ultrathin nanosheets for high energy density and flexible pseudocapacitors, *Nat. Commun.* **4** (2013) 2431.

19. V.V. Boldyrev, Reactivity Of Solids, *J. Thermal Anal.* **40** (1993) 1041.

20. H. L.C. Michalk, K. Knese, and P. Eichhorn, Thermal Decomposition of Freezedried Complex Acetates of Iron, Nickel and Zinc, and Structural Characterization of Products, *J. Eur. Ceram. Soc.* **8** (1991) 171.

21. X. Zhao, B. Zheng, C. Li, H. Gu, Acetate-derived ZnO ultrafine particles synthesized by spray pyrolysis, *Powder Technol.* **100** (1998) 20.

22. W.-S. Dong, F.-Q. Lin, C.-L. Liu, M.-Y. Li, Synthesis of ZrO2 nanowires by ionic-liquid route, *J. colloid interf. Sci.* **333** (2009) 734.

23. J.V. Bellini, S.N. de Medeiros, A.L.L. Ponzoni, F.R. Longen, M.A.C. de Melo, A. Paesano Jr., Manganese ferrite synthesized from Mn(II) acetate + hematite freeze-dried powders, *Materials Chemistry and Physics* **105** (2007) 92.

24. T. Nathan, M. Cloke, and S. R. S. Prabaharan, Electrode Properties of Mn2O3 Nanospheres Synthesized by Combined Sonochemical/Solvothermal Method for Use in Electrochemical Capacitors. *Journal of Nanomaterials*, **2008** (2008) 1-8.

25. B. Gillot, M. El Guendouzi, M. Laarj, Particle size effects on the oxidation-reduction behavior of Mn3O4 hausmannite, *Materials Chemistry and Physics* **70** (2001) 54.

26. M. Kahouli, A. Bouzid, A. Barhoumi, A. Al-Hajry, *Superlattice Microst.* **85** (2015) 7.

27. M. Miki-yoshida, Optical Band Gap Estimation of ZnO Nanorods, *Mater. Res. Suppl.* **19** (1) (2016) 33.

28. R. Peymani, R. Poursalehi, A. Yourdkhani, Optical and structural properties of colloidal zirconia nanoparticles prepared by arc discharge in liquid. *AIP Conference Proceedings* **1920** (2018).